Supplementary Materials for

Synthesis of Highly Dispersed Carbon-Encapsulated Ru-FeNi Nanocatalyst by Lignin-Metal Supramolecular Strategy for Durable Water-Splitting Electrocatalysis

Jianglin Liu 1, Xueqing Qiu1,2,3,, Shirong Sun1,*, Bowen Liu1, Yuhui Tian1, Yanlin Qin1, 2, 3, Xuliang Lin1, 2, 3,**

1Guangdong Provincial Key Laboratory of Plant Resources Biorefinery, School of Chemical Engineering and Light Industry, Guangdong University of Technology, Guangzhou 510006, China

2Guangdong Provincial Laboratory of Chemistry and Fine Chemical Engineering Jieyang Center, Jieyang 515200, China

3Guangdong Basic Research Center of Excellence for Ecological Security and Green Development, Guangdong University of Technology, Guangzhou 510006, China

1. Physicochemical characterization

The EHL and OAL (90 mg) were dissolved in 0.6 ml of DMSO-d6 for two-dimensional heteronuclear single quantum coherence nuclear magnetic resonance (2D HSQC NMR) analysis. An appropriate amount of chromium (III) acetylacetonate was added to facilitate the relaxation of magnetization. The experiments were performed on a 9.4 T Bruker Avance III 400 spectrometer equipped with a 5 mm BB probe operating at 400 MHz. Data with sufficient amounts of scans consisting of 4096 by 256 points were collected in order to reach a steady state and obtain clear spectra. 13C solid-state NMR spectra of EHL, OAL, and OAL-metal complex were recorded on a Bruker Advance 400 MHz NMR spectrometer equipped with a Bruker 4 mm CP/MAS solid-state probe and a magic angle spinning speed of 15 kHz. An FEI Tecnai G2 F20 transmission electron microscopy (TEM) instrument with a 200-kV voltage was used to characterize the morphology and elemental composition. A Rigaku Miniflex-600 X-ray diffraction (XRD) instrument with a Cu-Kα radiation X-ray source was used to characterize the crystal structure of the electrocatalyst at a scanning range and rate of "2θ = 5°–80°" and $10°\cdot min^{-1}$, respectively. An X-ray photoelectron spectrometer (Thermo Scientific K-Alpha) was used to characterize the elemental composition and valence state of Ru-FeNi@OALC catalyst. The peaks were calibrated according to the standard position of the C 1s peak (284.8 eV). The percentage of doped metal in the sample was calculated using inductively coupled plasma-optical emission spectrometry (ICP-OES, Varian 720).

2. Electrochemical measurements

Electrochemical measurements were performed in a three-electrode system using the Gamry Interface 1010 electrochemical workstation. A graphite rod and Hg/HgO were used as the counter and reference electrodes, respectively. The working electrode was prepared as follows. Approximately 4 mg of carbon powder was added into 200 μL of a 0.25% Nafion–ethanol solution. After an ultrasonic dispersion of the powder, 50 μL of the slurry was dropped onto the treated carbon paper and held using an

electrode clamp as the working electrode. The loading capacity of the catalyst was 4 $mg \cdot cm^{-2}$.

The electrochemical performances were investigated using linear sweep voltammetry (LSV) and cyclic voltammetry (CV) at room temperature. KOH solution (1 $mol \cdot L^{-1}$) was used as an electrolyte, and the scanning rate recorded by the polarization curves was 2 $mV \cdot s^{-1}$. The working electrode with the loading catalyst was initially activated by multiple CV cycles prior to the LSV. An ohmic potential (iR) drop was used to correct the polarization curve data, and the potentials were calculated using the reversible hydrogen electrode (RHE). The expression was as follows:

"E " ("vs.RHE")" = E " ("vs.Hg/HgO")" + 0.098 + 0.0591 × pH" .

The electrochemical impedance spectroscopy was performed with applied biases of 0.61 V (vs. Hg/HgO) and -0.97 V (vs. Hg/HgO) for OER and HER, respectively, and an additional alternating voltage at 5 mV and the frequency ranging from 0.1 Hz to 100 kHz.

3. Theoretical calculations

All-atom MD simulations were employed to investigate the structural characteristics of OAL-M, OAL-M networks contained 112 of OAL-Fe, 112 of OAL-Ni, and 11 of OAL-Ru, respectively. The number of clusters was chosen so that all three systems contained 100 Fe ions. Each oxidized carbonaceous molecule (i.e., soot particle) was built with side aromatic bearings with a chemical composition of C96H102O10. All systems were simulated in the NVT (constant number of atoms, volume, and temperature) ensemble at temperatures of 300 and 973 K in a cubic simulation cell of 55 × 55 × 55 Å3 with periodic boundary conditions. The equations of motion were integrated using the velocity–Verlet algorithm with a timestep of 1 fs. The transferable, extensible, accurate and modular (TEAM-FF) force field was employed for all three systems with partial charges assigned to each atom based on the bond increments method. The long-range coulombic interactions were computed by the particle–particle particle–mesh solver. All networks were simulated for 5 ns both at ambient and elevated temperatures.

The Vienna Ab Initio Simulation Package was used to perform density functional theory (DFT) calculations. The generalized gradient approximation with the spin-polarized Perdew–Burke–Ernzerhof (PBE) functional was used to characterize the exchange-correlation potential. The electron-ion interaction was described using the projector augmented wave, and the plane-wave energy cutoff was set to 400 eV. The structures were optimized using a convergence criterion of 1×10^{-5} eV for the energy and 0.01 eV/Å for the forces. A periodic 4 × 4 graphene support was also built. The vacuum spacing was set to more than 15 Å for surface isolation to prevent interactions between the two neighboring surfaces. Brillouin zone sampling was employed using a Monkhorst–Packing grid with 9 × 9 × 1 for the calculated models. Dense k-points (9 × 9 × 1) were used for the calculations of the density of states (DOSs). For a commercial Pt/C, we used a Pt (3 × 3) unit cell of Pt (111) surface models. The Pt (111) slab had four atom layers, and the top two layers were fully relaxed during the structural optimization. Geometry optimizations for Pt (111) were performed with a 4 × 4 × 1 k-mesh. For each elementary step, the Gibbs reaction free energy (ΔG) is the difference between the free energies of the initial and final states given by $\Delta G = \Delta E + \Delta ZPE - T\Delta S + \Delta GU + \Delta G_{pH}$, where ΔE is the reaction energy of the reactant and product molecules adsorbed on the catalyst surface, obtained using the DFT calculations and ΔZPE and ΔS are the change in zero-point energies and entropy due to the reaction. $\Delta GU = -neU$, where U is the electrode applied potential relative to the RHE, e is the elementary charge transferred, and n is the number of protons–electron pairs transferred. ΔG_{pH} is the correction of the H+ free energy ($\Delta G_{pH} = -k_B T \ln[H+] = pH \times k_B T \ln 10$).

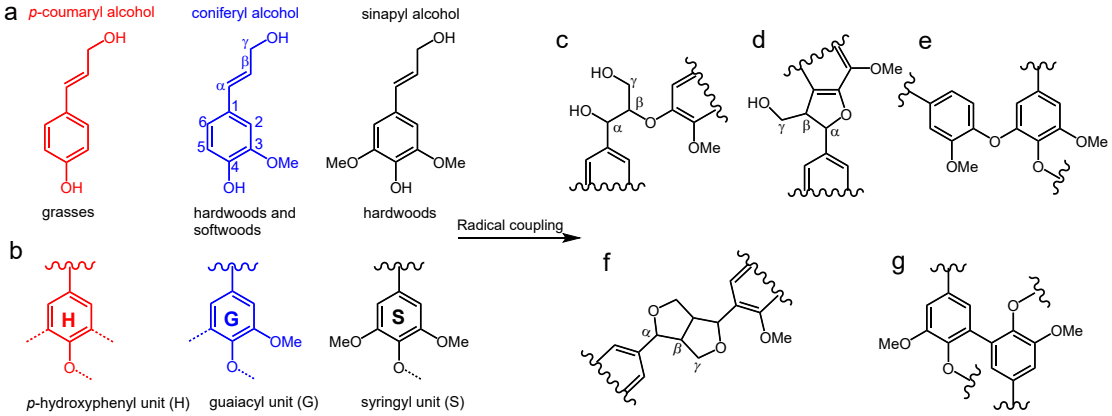

Figure S1. (a) Monomeric lignin precursors (monolignols) and (b) the corresponding general structural units in lignin. The most common covalent linkages of lignin: (c) β-aryl ether (β-O-4) (d) phenylcoumaran (β-5 (α-O-4)), (e) bifenyl ether (4-O-5), (f) bifenyl (5–5), (g) resinol (β–β (γ-O-4)).

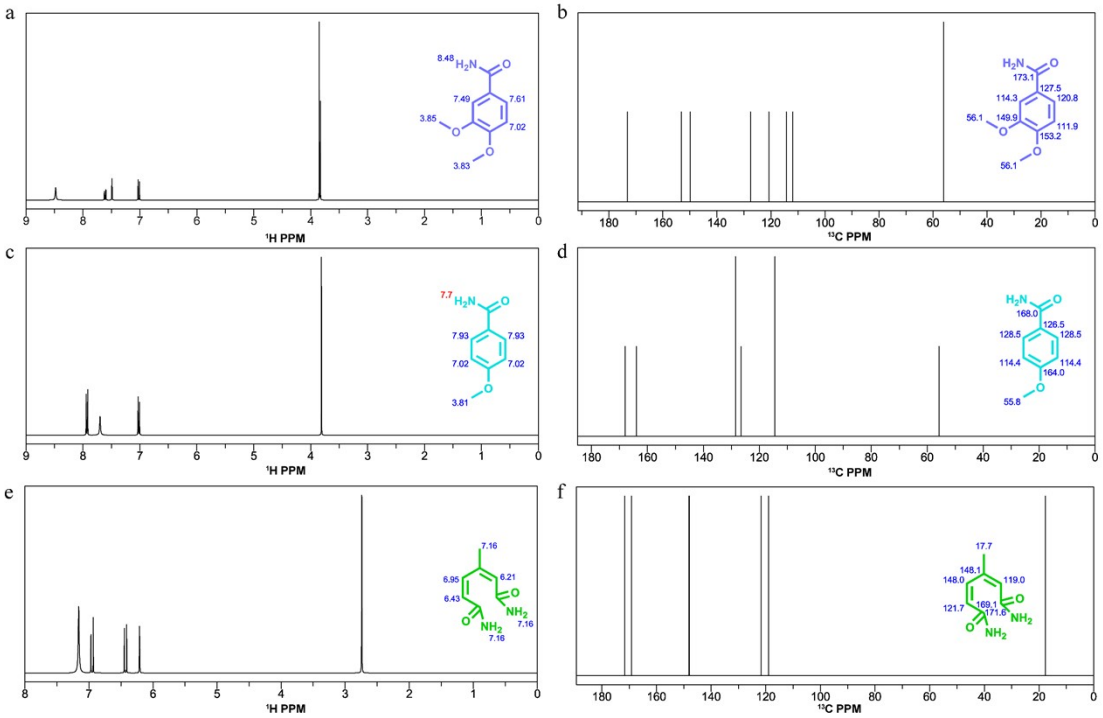

Figure S2. ChemNMR ^{1}H and ^{13}C estimation of the structure of GBa (a and b), *p*Ba (c and d), and Hda (e and f).

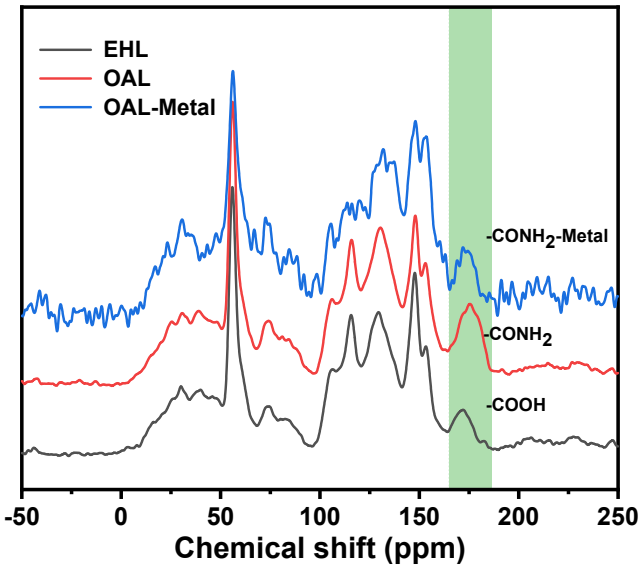

Figure S3. ^{13}C solid-state NMR spectra of EHL, OAL, and OAL-metal complex.

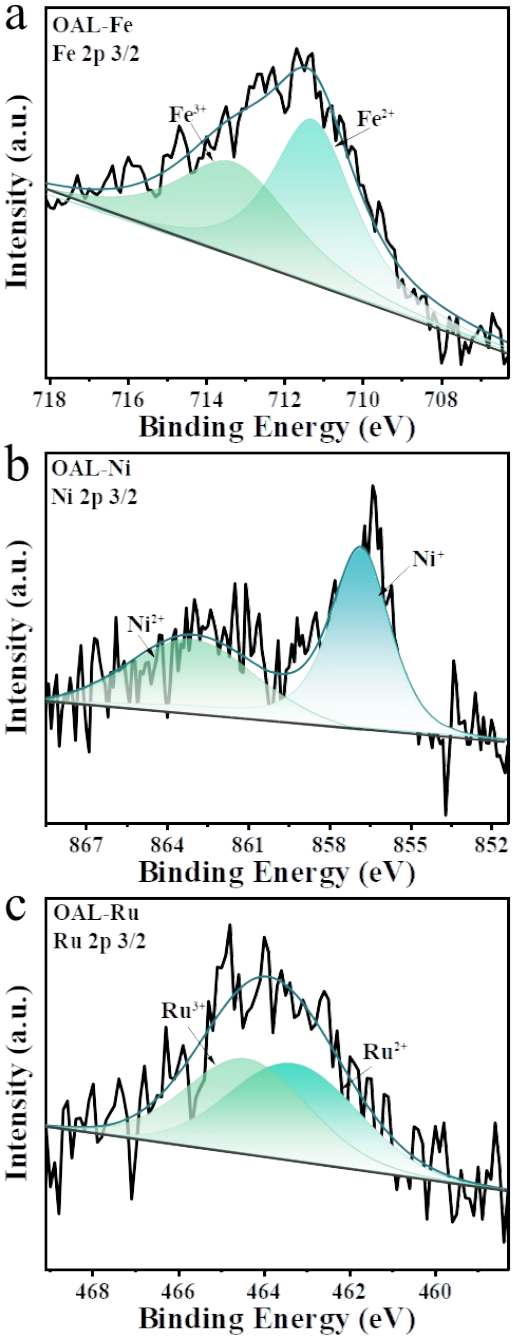

Figure S4. The Fe 2p, Ni 2p, and Ru 2p XPS spectra of the OAL-Metal supramolecular.

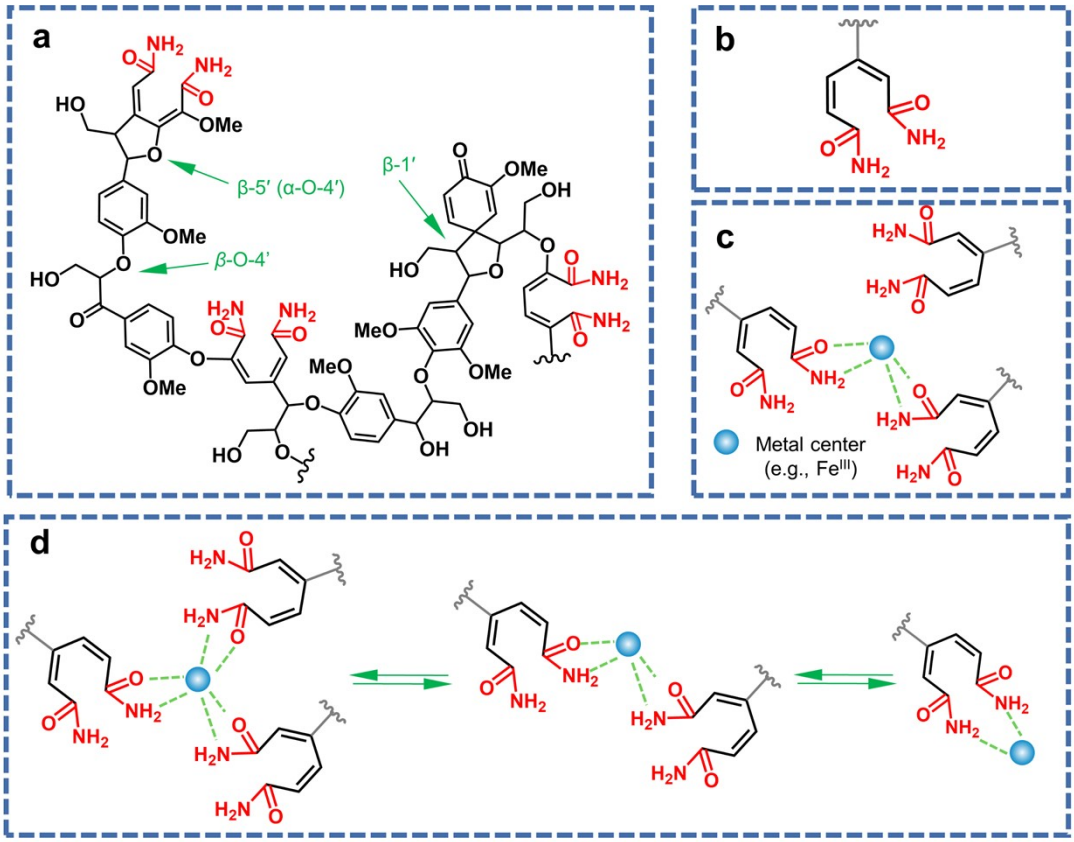

Figure S5. OAL and lignin-metal supramolecular chemistry. (a) Structure of the OAL. (b) Basic coordination center in OAL. (c) Coordination chemistry between the OAL and metal ions. (d) The prevalent formation of mono-, bis-, and tris-complexes in localized lignin-metal supramolecular with different metal ions.

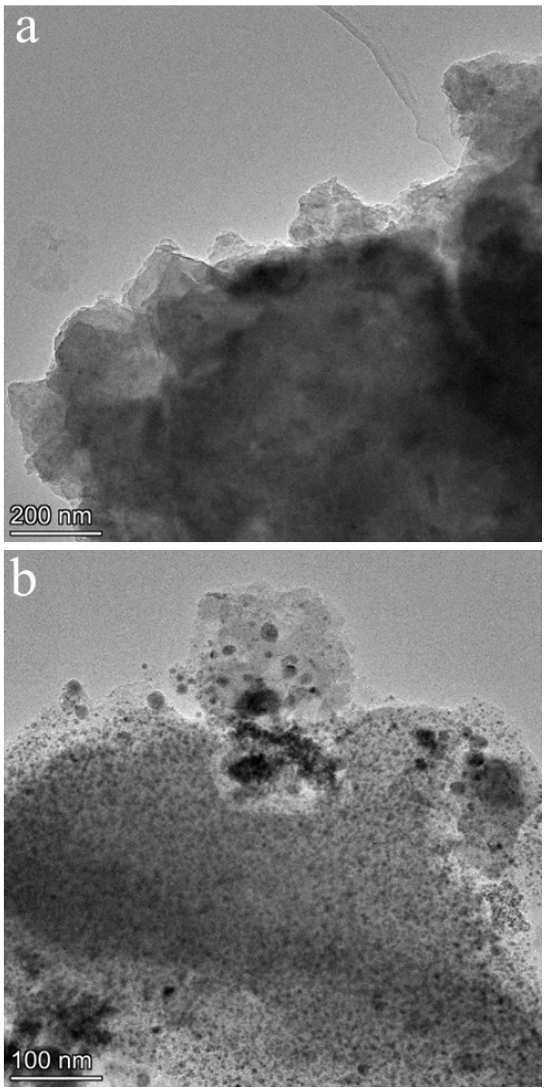

Figure S6. (a,b) TEM images of the Ru-FeNi@OALC catalyst.

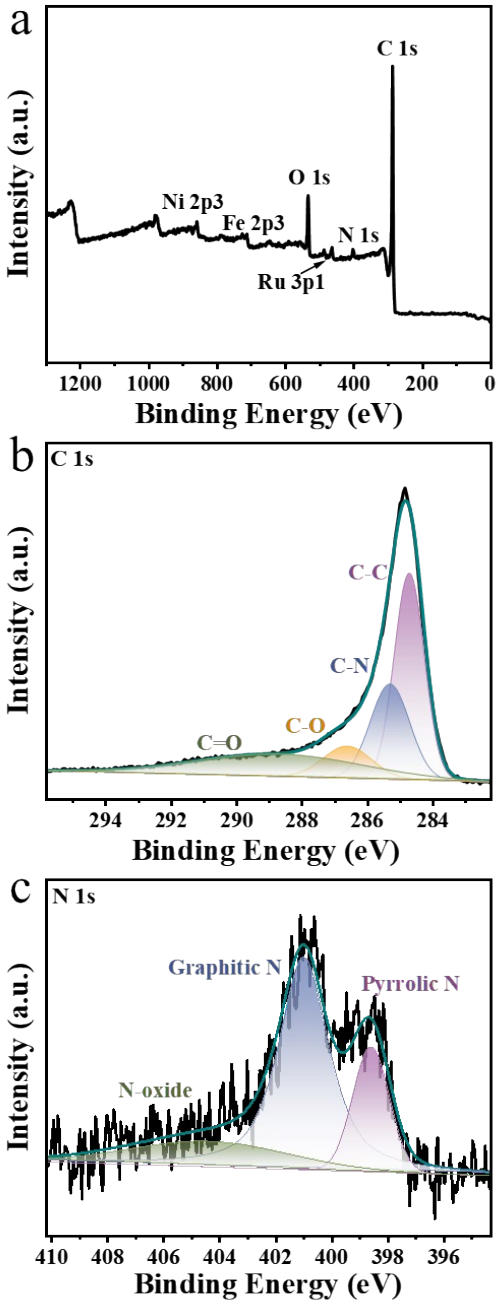

Figure S7. (a) XPS spectra Survey and high resolution (b) C 1s and (c) N 1s of the Ru–FeNi@OALC catalyst.

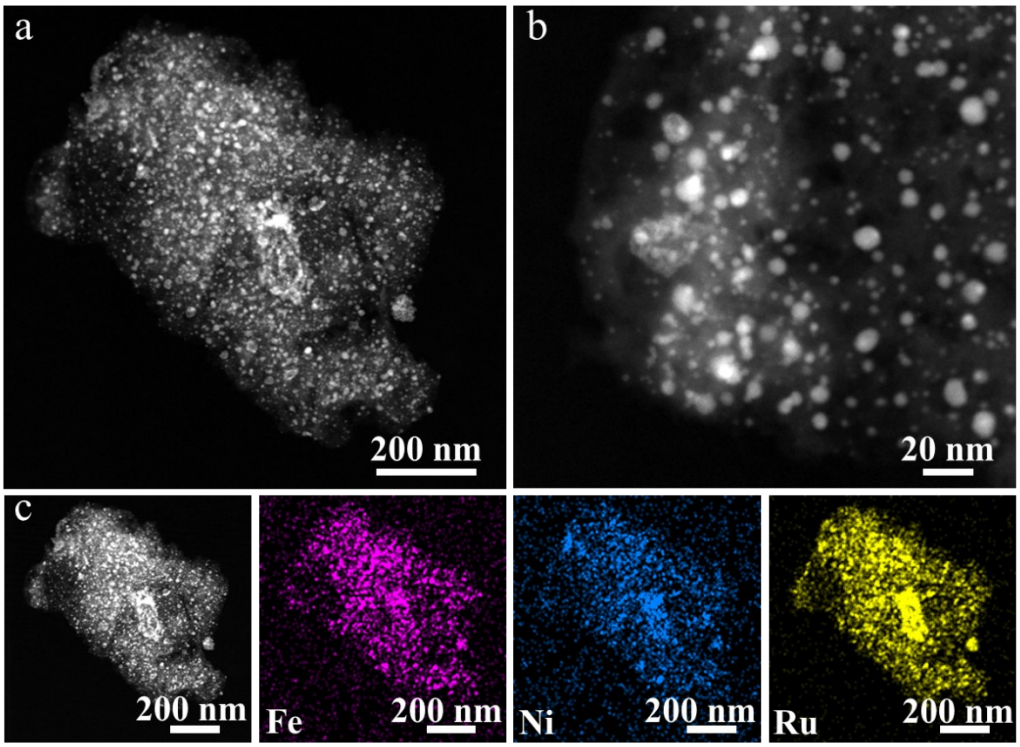

Figure S8. (a) transmission electron microscopy (TEM) image, (b) high-resolution (HRTEM) image, (c) HAADF-STEM image and corresponding EDS mappings of Ru–FeNi@OALC after the stability test of electrolyzed water.

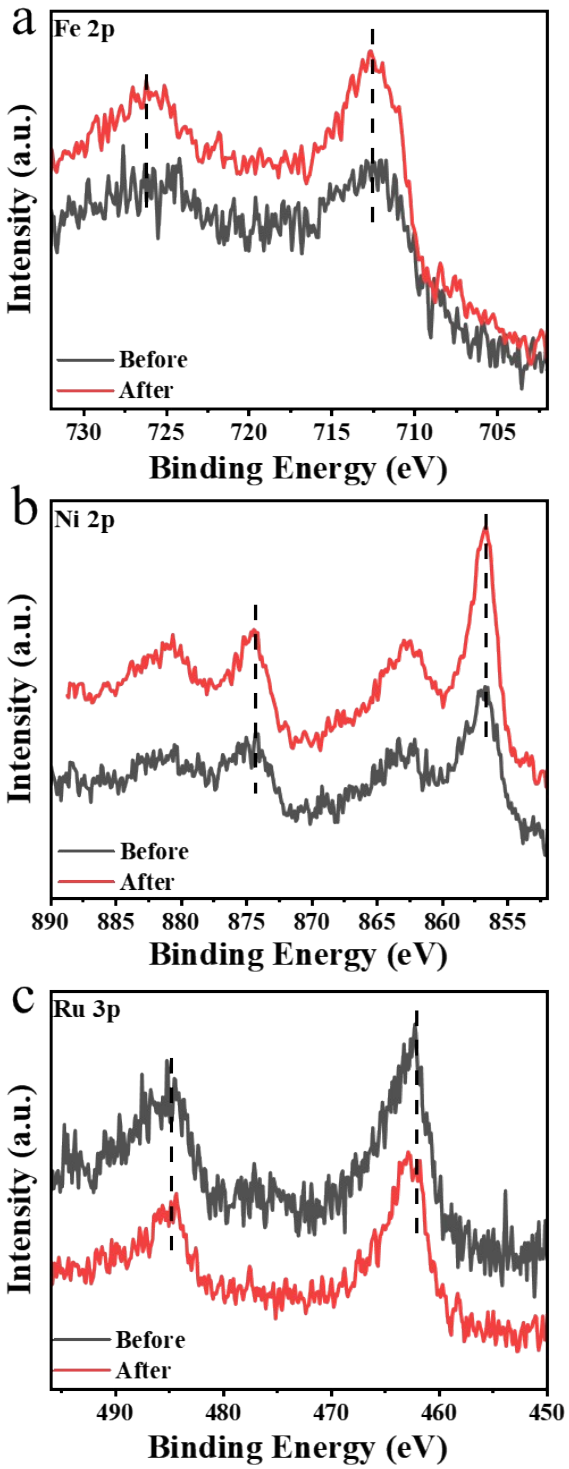

Figure S9. (a) Fe 3p XPS spectrum of Ru-FeNi@OALC. (b) Ni 2p XPS spectrum of Ru-FeNi@OALC. (c) Ru 3p XPS spectrum of Ru-FeNi@OALC after the stability test of electrolyzed water.

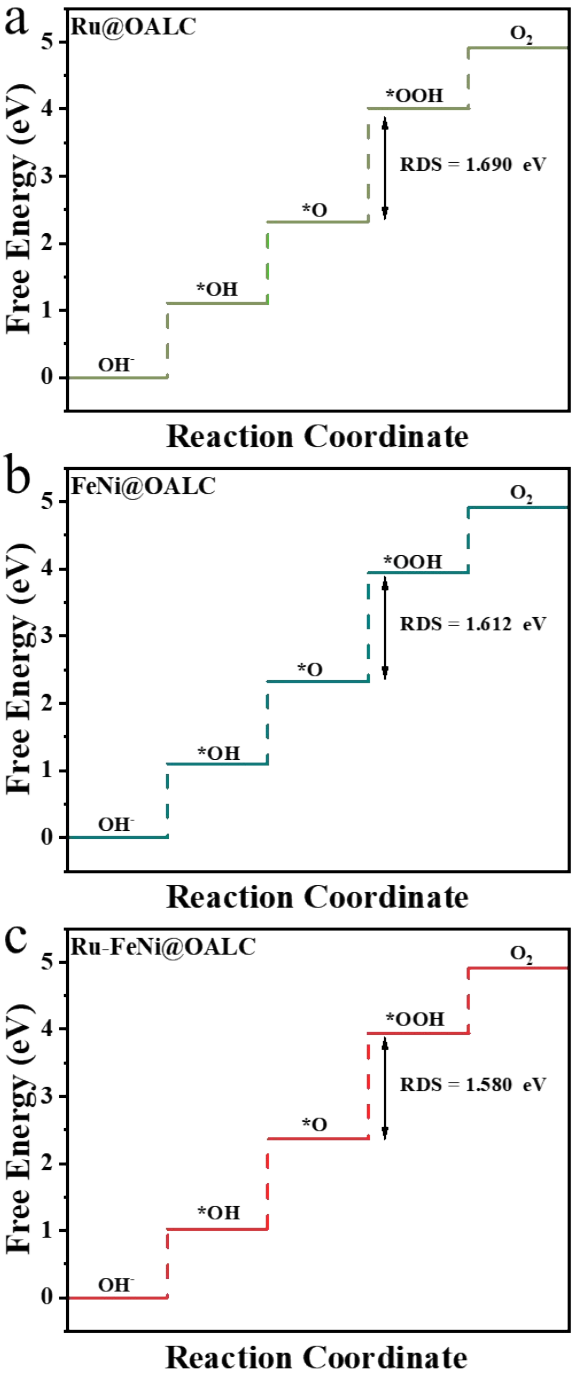

Figure S10. (a)-(c) Gibbs free energy curves of OER on Ru@OALC, FeNi@OALC, and Ru-FeNi@OALC at 0 V.

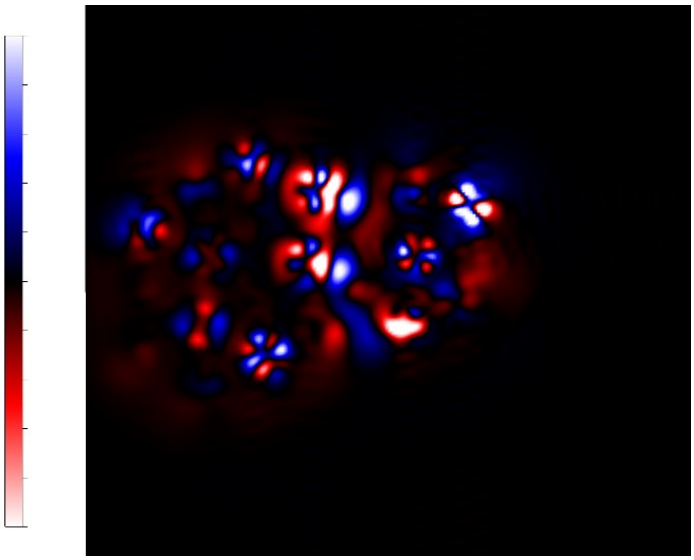

Figure S11 Difference in charge density of Ru–FeNi@OALC.

Table S1. ChemNMR 1H 13C Estimation of the structure of GBa

	Node	Shift	Base + Inc.	Comment (ppm rel. to TMS)
	NH2	8.48	7.00	sec. amideC
			0.70	1 -1:C*C*C*C*C*C*1
			0.78	general corrections
	CH	7.49	7.26	1-benzene
			-0.38	1 -O-C
			0.00	1 -O-C
			0.69	1 -C(=O)N
			-0.08	general corrections
	CH	7.02	7.26	1-benzene
Protocol of the			0.00	1 -O-C
H-1 NMR			-0.38	1 -O-C
Prediction			0.18	1 -C(=O)N
(Lib=SU			-0.04	general corrections
Solvent=DMSO	CH	7.61	7.26	1-benzene
300 MHz)			-0.32	1 -O-C
			0.00	1 -O-C
			0.69	1 -C(=O)N
			-0.02	general corrections
	CH3	3.85	0.86	methyl
			2.87	1 alpha -O-1:C*C*C*C*C*C*1
			0.12	general corrections
	CH3	3.83	0.86	methyl
			2.87	1 alpha -O-1:C*C*C*C*C*C*1
		8.48	0.10	general corrections
	shift	atom index	coupling partner	constant and vector
	8.48	9		
	7.49	4		
1H NMR			8	1.5 H-C*C*C-H
Coupling	7.02	7		
Constant			8	7.5 H-C*C-H
Prediction	7.61	8	7	7.5 H-C*C-H
			4	1.5 H-C*C*C-H
	3.85	13		
	3.83	11		

Table S2. ChemNMR 13C Estimation of the structure of GBa

	Node	Shift	Base + Inc.		Comment (ppm rel. to TMS)
	C	149.9	128.5		1-benzene
				33.5	1 -O-C
				-14.4	1 -O-C
				0.1	1 -C(=O)-N
				2.2	general corrections
	C	153.2	128.5		1-benzene
				-14.4	1 -O-C
				33.5	1 -O-C
				3.4	1 -C(=O)-N
				2.2	general corrections
	C	127.5	128.5		1-benzene
				1.0	1 -O-C
				-7.7	1 -O-C
				5.0	1 -C(=O)-N
				0.7	general corrections
	CH	114.3	128.5		1-benzene
				-14.4	1 -O-C
				1.0	1 -O-C
				-1.2	1 -C(=O)-N
Protocol of the C-13 NMR Prediction: (Lib=S)				0.4	general corrections
	CH	111.9	128.5		1-benzene
				1.0	1 -O-C
				-14.4	1 -O-C
				0.1	1 -C(=O)-N
				-3.3	general corrections
	CH	120.8	128.5		1-benzene
				-7.7	1 -O-C
				1.0	1 -O-C
				-1.2	1 -C(=O)-N
				0.2	general corrections
	C	173.1	165.0		1-amide
				4.7	1 -1:C*C*C*C*C*C*1
				3.4	general corrections
	CH3	56.1	-2.3		aliphatic
				49.0	1 alpha -O
				9.3	1 beta -1:C*C*C*C*C*C*1
				0.3	1 delta -O
				-0.2	general corrections
	CH3	56.1	-2.3		aliphatic
				49.0	1 alpha -O
				9.3	1 beta -1:C*C*C*C*C*C*1
				0.3	1 delta -O
				-0.2	general corrections

Table S3. ChemNMR 1H Estimation the structure of *p*Ba

	Node	Shift	Base + Inc.	Comment (ppm rel. to TMS)
	NH2	7.7	7.00	sec. amideC
			0.70	1 -1:C*C*C*C*C*C*1
	CH	7.02	7.26	1-benzene
			-0.38	1 -O-C
			0.18	1 -C(=O)N
			-0.04	general corrections
	CH	7.93	7.26	1-benzene
Protocol of the H-1 NMR Prediction (Lib=SU Solvent=DMSO 300 MHz)			0.00	1 -O-C
			0.69	1 -C(=O)N
			-0.02	general corrections
	CH	7.02	7.26	1-benzene
			-0.38	1 -O-C
			0.18	1 -C(=O)N
			-0.04	general corrections
	CH	7.93	7.26	1-benzene
			0.00	1 -O-C
			0.69	1 -C(=O)N
			-0.02	general corrections
	CH3	3.81	0.86	methyl
			2.87	1 alpha -O-1:C*C*C*C*C*C*1
			0.08	general corrections
	shift	atom index	coupling partner,	constant and vector
	7.7	9		
	7.02	5		
			4	7.5 H-C*C-H
			7	1.5 H-C*C*C-H
	7.93	4		
1H NMR Coupling Constant Prediction			5	7.5 H-C*C-H
			8	1.5 H-C*C*C-H
	7.02	7		
			8	7.5 H-C*C-H
			5	1.5 H-C*C*C-H
	7.93	8		
			7	7.5 H-C*C-H
			4	1.5 H-C*C*C-H
	3.81	11		

Table S4. ChemNMR 13C Estimation the structure of *p*Ba

	Node	Shift	Base+Inc .		Comment (ppm rel. to TMS)
	C	164.0	128.5		1-benzene
				33.5	1 -O-C
				3.4	1 -C(=O)-N
				-1.4	general corrections
	C	126.5	128.5		1-benzene
				-7.7	1 -O-C
				5.0	1 -C(=O)-N
				0.7	general corrections
	CH	114.4	128.5		1-benzene
				-14.4	1 -O-C
				0.1	1 -C(=O)-N
				0.2	general corrections
	CH	128.5	128.5		1-benzene
Protocol				1.0	1 -O-C
of the C-				-1.2	1 -C(=O)-N
13 NMR				0.2	general corrections
Prediction:	CH	114.4	128.5		1-benzene
(Lib=S)				-14.4	1 -O-C
				0.1	1 -C(=O)-N
				0.2	general corrections
	CH	128.5	128.5		1-benzene
				1.0	1 -O-C
				-1.2	1 -C(=O)-N
				0.2	general corrections
	C	168.0	165.0		1-amide
				4.7	1 -1:C*C*C*C*C*C*1
				-1.7	general corrections
	CH3	55.8	-2.3		aliphatic
				49.0	1 alpha -O
				9.3	1 beta -1:C*C*C*C*C*C*1
				-0.2	general corrections

Table S5. ChemNMR 1H Estimation of the structure of Hda

	Node	Shift	Base + Inc.		Comment (ppm rel. to TMS)
Protocol of the H-1 NMR Prediction (Lib=SU Solvent=DMSO 300 MHz):	NH2	7.16	7.00		sec. amideC
				0.20	1 -C=C
				-0.04	general corrections
	NH2	7.16	7.00		sec. amideC
				0.20	1 -C=C
				-0.04	general corrections
	CH3	2.74	0.86		methyl
				1.15	1 alpha -C=C-C=O
				0.73	general corrections
	H	6.21	5.25		1-ethylene
				-0.05	1 -C=C trans
				-0.22	1 -C cis
				1.23	1 -C(=O)N gem
	H	6.43	5.25		1-ethylene
				1.23	1 -C(=O)N gem
				-0.05	1 -C=C trans
	H	6.95	5.25		1-ethylene
				0.46	1 -C(=O)N trans
				1.24	1 -C=C gem

1H NMR Coupling Constant Prediction	shift	atom index	coupling partner,	constant and vector
	7.16	11		
	7.16	10		
	2.74	2		
			12	-1.0 H-CH2>C=C<H
	6.21	12		
			2	-1.0 H>C=C<CH2-H
	6.43	13		
			14	10.9 H>C=C<H
	6.95	14		
			13	10.9 H>C=C<H

Table S6. ChemNMR 13C Estimation of the structure of Hda

	Node	Shift	Base+Inc.		Comment(ppm rel. to TMS)
	C	169.1	165.0		1-amide
				2.6	1 -C=C-C
				1.5	general corrections
	C	171.6	165.0		1-amide
				3.3	1 -C=C
				3.3	general corrections
	C	148.1		123.3	1-ethylene
				13.6	1 -C=C
				9.4	1 -C
				5.8	1 -C(=O)N
				-4.0	general corrections
Protocol of the C-13 NMR Prediction: (Lib=S)	CH	119.0	123.3		1-ethylene
				-7.0	1 -C=C
				-7.4	1 -C
				7.5	1 -C(=O)N
				2.6	general corrections
	CH	121.7	123.3		1-ethylene
				7.5	1 -C(=O)N
				-7.0	1 -C=C
				-2.1	general corrections
	CH	148.0	123.3		1-ethylene
				5.8	1 -C(=O)N
			13.6		1 -C=C
				5.3	general corrections
	CH3	17.7	-2.3		aliphatic
				19.5	1 alpha -C=C
				6.9	1 beta -C=C
				-3.2	1 gamma -C(=O)-N
				-0.4	1 delta -C(=O)-N
				-2.8	general corrections

Table S7 Comparison of HER, OER and total water splitting performance of Ru-FeNi@OALC with similar catalysts reported in literature.

Catalyst	HER		OER		Cell voltage (V)	Ref.
	η_{10}, mV	Tafel slope	η_{10}, mV	Tafel slope	10 mA/cm^2	
Ru@FeCoP	11	31.6	212	45.7	1.56	[1]
Ni-Ru@Fe/C@CNT	32	54	246	31	1.57	[2]
Ru-CoNi@NC	268	63	240	75	1.57	[3]
$RuNi_1Co_1$@CMT	78	77	299	83	1.58	[4]
NiFeP/CF	282	125	273	55	1.59	[5]
$Ru_{0.7}Co_{0.3}$ aerogel	42	41.6	272	72.1	1.59	[6]
Ni_3FeN/r-GO	94	90	270	54	1.60	[7]
MIL-53(Ru-NiFe)@NF	62	49	210	42	1.60	[8]
RuNi-Fe_2O_3/IF	75	85	329	61	1.66	[9]
Ru-G/CC	40	76	270	63	1.67	[10]
Ru-FeNi@OALC	52	46	290	108	1.56	This work

1. Y. Wang, Y. Du, Z. Fu, J. Ren, Y. Fu and L. Wang, *J. Mater. Chem. A*, 2022, **10**, 16071-16079.
2. T. Gao, X. Li, X. Chen, C. Zhou, Q. Yue, H. Yuan and D. Xiao, *Chem. Eng. J.*, 2021, **424**, 130416.
3. W. Wang, S. Xi, Y. Shao, W. Sun, S. Wang, J. Gao, C. Mao, X. Guo and G. Li, *ACS Sustainable Chem. Eng.*, 2019, **7**, 17227-17236.
4. Y. Xue, Q. Yan, X. Bai, Y. Xu, X. Zhang, Y. Li, K. Zhu, K. Ye, J. Yan, D. Cao and G. Wang, *J. Colloid Interface Sci.*, 2022, **612**, 710-721.
5. H. Huang, C. Yu, C. Zhao, X. Han, J. Yang, Z. Liu, S. Li, M. Zhang and J. Qiu, *Nano Energy*, 2017, **34**, 472-480.
6. L. Zongshan, L. Shilong, L. Yonggang, L. Zhe, Z. Shuidong, Z. Xiaofeng, T. Yong and T. Zhenghua, *J. Power Sources*, 2021, **514**, 230600.
7. Y. Gu, S. Chen, J. Ren, Y. A. Jia, C. Chen, S. Komarneni, D. Yang and X. Yao, *ACS Nano*, 2018, **12**, 245-253.
8. Z. Ming, L. Huilin, L. Wei, L. Junying, Y. Lingya, H. Weihua and L. Chang Ming, *Chemistry - A European Journal*, 2020, **26**, 17091-17096.
9. C. Tong, Z. Xuejun, G. Lili, C. Jing-Qi, Z. Yu, Z. Jiawei, S. Xuemei and W. Lei, *Chin. J. Catal.*, 2022, **43**, 2202-2211.
10. Y. Mingzhu, D. Xin, H. Xinghui, W. Zeyuan, Z. Ying, J. Haipeng, Z. Liying, Z. Zongtao, Y. Shasha and C. Deliang, *Appl. Catal., B*, 2022, **317**, 121729.